Thin Solid Films 519 (2011) 4969–4973

Contents lists available at ScienceDirect

Thin Solid Films

journal homepage: www.elsevier.com/locate/tsf

Properties of polyimide/Al_2O_3 and Si_3N_4 deposited thin films

Mei-Hui Tsai [a,*], Hong-Yi Wang [a], Hsu-Tung Lu [a], I-Hsiang Tseng [a], Hung-Hua Lu [b], Shih-Liang Huang [a], Jui-Ming Yeh [c]

[a] Department of Chemical and Materials Engineering, National Chin-Yi University of Technology, Taichung 41111, Taiwan, ROC
[b] Department of Mechanical Engineering, National Chin-Yi University of Technology, Taichung 41111, Taiwan, ROC
[c] Department of Chemistry, Center for Nanotechnology at CYCU, Chung-Yuan Christian University, Chung Li32023, Taiwan, ROC

ARTICLE INFO

Available online 14 January 2011

Keywords:
Polyimide/Al_2O_3 hybrid
Silicon nitride
Water vapor transmission rate
RF magnetron sputtering

ABSTRACT

Polyimide (PI) nanocomposites with different proportions of Al_2O_3 were prepared via two-step reaction. Silicon nitride (Si_3N_4) was deposited on PI composite films by a RF magnetron sputtering system and used as a gas barrier to investigate the water vapor transmission rate (WVTR). The thermal stability and mechanical properties of a pure PI film can be improved obviously by adding adequate content of Al_2O_3. At lower sputtering pressure (4 mTorr), the PI/Al_2O_3 hybrid film deposited with Si_3N_4 barrier film exhibits denser structure and lower root mean square (RMS) surface roughness (0.494 nm) as well as performs better in preventing the transmission of water vapor. The lowest WVTR value was obtained from the sample, 4 wt.% Al_2O_3–PI hybrid film deposited with Si_3N_4 barrier film with the thickness of 100 nm, before and after bending test. The interface bonding, Al–N and Al–O–Si, was confirmed with the XPS composition-depth profile.

1. Introduction

The applications of gas barrier in the flexible plastic displays have been reported by many researchers in recent years. Flexible electronic device or substrate is a prerequisite for the appearance of flexible displays due to the requirement of being lighter, thinner, shorter, smaller, more flexible, and roll-to-roll process. Usually plastic materials are requisite materials in flexible displays, solar cells and illumination devices due to their excellent optical transparency. However, glass substrates with plastic contents will be a huge challenge owing to the absence of thermal and dimensional stability [1].

The sol-gel method has been widely used to develop nanoscale inorganic oxide particles in a polymer matrix to enhance the thermal and dimensional stability of polymer materials [2–8]. In addition, the addition of nanosized metal oxide particles in PI matrix increases the moving path of water vapor in polymer matrix and in consequence decreases the water vapor transmission rate [9].

Although the applications of flexible plastic displays have been reported by many researchers, no flexible plastic materials possess both water vapor and oxygen barriers. Moreover, the inorganic film is a better water vapor barrier than the organic film. For this reason, the use of inorganic oxide coatings as a gas barrier film on polymers has attracted a considerable amount of interest. Gas barrier films such as aluminium oxide, silicon oxide, aluminium nitride, silicon nitride, titanium oxynitride and aluminiumoxynitride with the coating thickness ranging from 1 to 1000 nm have been widely investigated [10–19]. Plasma enhanced chemical vapor deposition and reactive magnetron sputtering have been employed to deposit inorganic oxide films on polymer substrates as gas barrier. Magnetron sputtering has been one of the multitude choices among those plasma techniques as a result of simple operation, low deposition temperature and less environmental hazard.

In this study, we prepared PI/Al_2O_3 hybrids with Si_3N_4 deposited thin films and investigated the water vapor transmission rate (WVTR). The PI/Al_2O_3 hybrids were based on monomers, ODA and ODPA and with different Al_2O_3 content. Silicon nitride was deposited on PI/Al_2O_3 hybrid films by RF magnetron sputtering system. The related properties and morphology of the composite films are also discussed in this paper.

2. Experimental

2.1. Materials

3,3′-oxydiphalic anhydride (ODPA) was purchased from industrial sources and dried before use. 4,4′-diaminodiphenyl ether (ODA) and aluminum 2,4-pentanedionate ($Al(acac)_3$) were commercial analytical grade reagents and purchased from TCI. N,N-dimethyl acetyamide (DMAc) as a solvent was dried over molecular sieves before use. A silicon nitride (Si_3N_4) target with the diameter of 3 in. and the purity of 99.9% was used.

* Corresponding author. Tel.: +886 4 23924505x7510; fax: +886 4 23926617.
E-mail address: tsaimh@ncut.edu.tw (M.-H. Tsai).

0040-6090/$ – see front matter © 2011 Elsevier B.V. All rights reserved.
doi:10.1016/j.tsf.2011.01.063

Table 1
RF magnetron sputtering conditions for Si_3N_4 barrier films.

Target	Si_3N_4 target with diameter of 3 in.
Substrates	Pure PI and PI/Al_2O_3 hybrid films
RF power	100 W
Base pressure	1.5×10^{-5} Torr
Work pressure	4 mTorr, 6 mTorr, 8 mTorr

2.2. Preparation of PI/Al_2O_3 hybrid films

The PI/Al_2O_3 hybrid films based on monomers, ODPA and ODA, and different amounts of Al_2O_3 were synthesized via in situ polymerization. A three-neck flask (100 ml) was first purged with nitrogen to remove the moisture before adding reagents. Then, 2.2627 g of ODA (11.3 mmol) and 12.25 g of dried DMAc were stirring mixed in the three-neck flask under nitrogen at room temperature for approximately 0.5 h to completely dissolve ODA in DMAc. Next, 3.5054 g of ODPA (11.3 mmol) and 5 g of DMAc were added in four-portion into the above solution. The mixture kept stirring at room temperature for 3 h under nitrogen to obtain a viscous poly(amic acid) (PAA) solution with the solid content of 23 w/wt.%. After then, 1.0147 g of Al $(acac)_3$ powder was added into DMAc and dispersed by ultrasonic treatment to get a saturated solution. This saturated solution was mixed with the above PAA solution and stirred for 10 h under nitrogen to obtain a homogenous and viscous PAA/Al_2O_3 solution. Then, the PAA/Al_2O_3 solution was cast on glass plates and followed by successively step-heating at 110, 170, 230 and 300 °C, each for 1 h. The PI hybrid film with 15 wt.% of Al_2O_3 was obtained. A series of PI hybrid films with Al_2O_3 content of 0, 2, 4, 6 and 10 wt.% were prepared through a similar procedure. The thickness of PI/Al_2O_3 films was ranging from 18 to 23 μm. In this paper, the sample code is presented by X-Al_2O_3–PI, where X implies the theoretically calculated weight percentage of Al_2O_3 within PI/Al_2O_3 matrix.

2.3. Preparation of Si_3N_4 barrier films

The Si_3N_4 films were deposited on PI/Al_2O_3 hybrid films by means of a RF magnetron sputtering system in which a silicon nitride disk was used as the target. Table 1 lists the sputtering conditions for Si_3N_4.

2.4. Measurements

The water vapor transmission rate (WVTR) of samples with the size of 10 cm^2 was measured using a Permatran-w 3/61 model system at atmospheric pressure, 40 °C and 100% relative humidity. The thickness of the deposited films was measured with an alpha-step profiler (Kosaka ET 4000a). The morphology of thin films was carried out with an atomic force microscope (AFM, Digital Instruments Nanoscope III) with multi-mode head. Tapping mode was employed by using Nanosensors silicon tips with the resonance frequency of 130 kHz. Scanning was accomplished with a scanning rate of 1 Hz and an image resolution of 512 × 512 pixels. Scanning electron microscopy (SEM) was performed on a JEOL JSM-6700F field emission scanning electron microscope using film samples coated with platinum. The dynamic mechanical analysis (DMA) was performed with a Dupont DMA 2980 at a frequency of 1 Hz, from 60 °C to 350 °C and with a heating rate of 3 °C/min. Thermogravimetric analysis (TGA) was carried out with a TA Q500 at a heating rate of 20 °C/min under nitrogen. The measurement of the in-plane coefficient of thermal expansion (CTE) of samples was carried out on a TA Q400 at a heating rate of 10 °C/min from 30 °C to 350 °C. The CTE of polymer was determined over a range of 30–240 °C. XPS spectra were obtained by using an X-ray photoelectron spectroscopy (ESCA PHI 5000).

Table 2
Properties of PI/Al_2O_3 hybrid films with different Al_2O_3 content.

Al_2O_3 content (wt.%)	TGA		DMA		CTE[c]
	Td_5 (°C)	Td_{10} (°C)	Tg[a] (°C)	E'[b] (MPa)	(ppm/°C)
0	579	594	272	1880	51.89
2	576	588	275	2003	47.31
4	574	588	280	2093	47.05
6	569	587	286	2140	47.00
10	568	588	301	2155	43.18
15	571	592	325	2059	41.33

[a] The maxiums in Tan δ curve was designated as Tg.
[b] Storage modulus of hybrid films was measured at 60 °C.
[c] The coefficient of thermal expansion (CTE) was determined over a range of 30–240 °C.

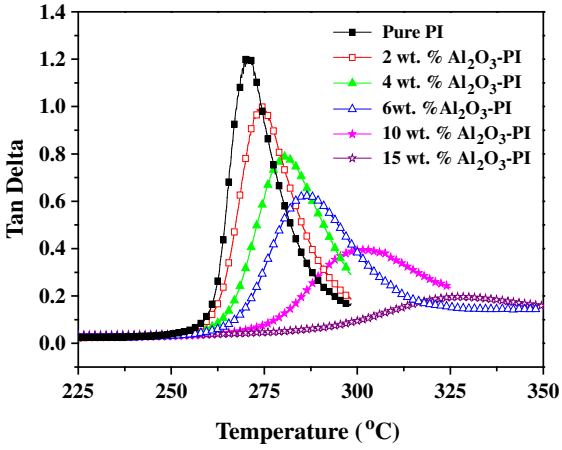

Fig. 1. The tan delta curves of pure polyimide and the hybrid films with various Al_2O_3 content.

3. Results and discussion

TGA, DMA and TMA were applied to characterize the decomposition temperature (Td_5), the glass transition temperature (Tg), the storage modulus and the CTE of PI/Al_2O_3 hybrid films. The TGA results (Table 2) were obtained to evaluate the thermal stability of PI/Al_2O_3 hybrid films. The decomposition temperature (Td_5), where 5 wt % weight loss occurs, of pure PI film was 579 °C. The Td_5 slightly decreased to 576, 574, 569, 568, and 571 °C corresponding to the hybrid films with Al_2O_3 content of 2, 4, 6, 10, and 15 wt.%, respectively. It reveals that the thermal stability of hybrid films was maintained while Al_2O_3 was incorporated with PI films.

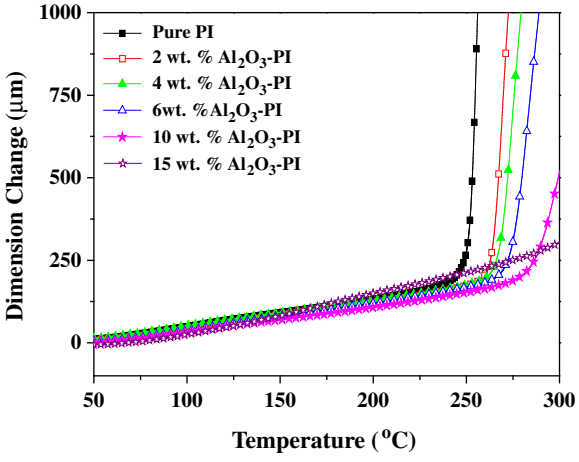

Fig. 2. The coefficient of thermal expansion (CTE) curves of pure polyimide and the hybrid films with various Al_2O_3 content.

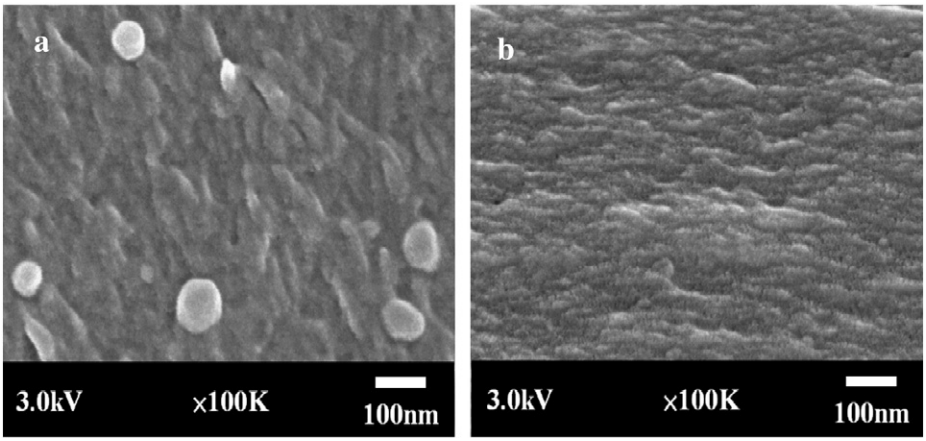

Fig. 3. Morphology of fractured surface of (a) 15 wt.% Al_2O_3–PI, and (b) pure PI by SEM.

Fig. 1 illustrates the temperature dependence of the tan delta (tan δ) for pure PI film and hybrid films. It is found that the Tg of the PI hybrid films increases gradually with the increase of Al_2O_3 content. They are located at 272, 275, 280, 286, 301, and 326 °C corresponding to the Al_2O_3 content of 0, 2, 4, 6, 10, and 15 wt.%, respectively. It seems that the movement of PI molecular chains is confined in the rigid structure of Al_2O_3, leading to an increase in Tg.

The storage modulus (E′) measured at 60 °C of the PI hybrid films with different Al_2O_3 content was listed in Table 2. The E′ value of hybrid films increased remarkably from 1880, 2003, 2093, 2140, and 2155 to 2059 MPa with the increase of Al_2O_3 content ranging from 0 to 15 wt.%. It is well known that good mechanical properties can be maintained by incorporation of the Al_2O_3 content. However, the storage modulus of the hybrid film decreased slightly as the Al_2O_3 content reached to 15 wt.%. It was believed that the aggregation of Al_2O_3 particles within PI matrix with high Al_2O_3 content contributes to the decrease in storage modulus.

The effect of Al_2O_3 content on the CTE of the PI hybrid films was also demonstrated in Fig. 2. The CTE of the PI hybrid films decreased gradually with the increase of Al_2O_3 content. The 15 wt.% Al_2O_3–PI had a CTE of 41 ppm/°C, in the temperature range of 30–240 °C, which was 24% lower than that of pure PI film. This dramatic decrease in CTE could be due to the low-CTE feature of inorganic materials (Al_2O_3). Besides, the network structure of Al_2O_3 domains could lead to the decrease in the segmental mobility of the polyimide chains. The reduced CTE value of PI/Al_2O_3 hybrid film could improve the existed thermal stress between Si_3N_4 barrier film and PI/Al_2O_3 hybrid film, and then reduce the separation of Si_3N_4 barrier film from PI/Al_2O_3 hybrid film.

Fig. 3 shows the FE-SEM photographs of the fracture surfaces of pure PI and 15 wt.% Al_2O_3–PI. A smooth surface was presented for the pure PI, in contrary, the dispersed Al_2O_3 particles with the size of 60 to 90 nm were revealed for 15 wt.% Al_2O_3–PI films.

Fig. 4 shows the root mean square (RMS) surface roughness of Si_3N_4 barrier films deposited in pure PI films at various working pressure. It is found that the RMS of surface roughness of the pure PI films increased with the increase of the work pressure. The RMS surface roughness increased to 0.494, 0.693, and 0.749 nm corresponding to the working pressure of 4, 6, 8 mTorr, respectively. In addition, the FE-SEM micrographs of Si_3N_4 barrier films deposited at various work pressure, 4 and 8 mTorr, are shown in Fig. 5. The results showed that the Si_3N_4 barrier films deposited at lower work pressure have a denser structure. A higher working pressure indicates a shorter mean free path and a higher collision probability of particles to lose their kinetic energy. The particles with lower kinetic energy will move slower on the surface of the PI film and a loose structure will deposit on the surface of pure PI at higher working pressure [6]. Therefore, the particles that maintain enough energy are important from deposition mechanism of barrier films.

The WVTR of Si_3N_4 deposited PI films in dependence of various work pressure is shown in Fig. 5. The WVTR of pure PI was 136.45 g/m^2-day. It can be found that the WVTR increased as working pressure increased from 4 mTorr to 8 mTorr. The WVTR was 1.18, 5.14 and 10.11 g/m^2-day corresponding to 4, 6 and 8 mTorr of working pressure. The increase in WVTR with working pressure was mainly caused by the decrease in the deposition rate and probably also by the increase of roughness. Moreover, the denser structure, which was proved by FE-SEM, of deposited film is usually thought to exhibit better barrier properties.

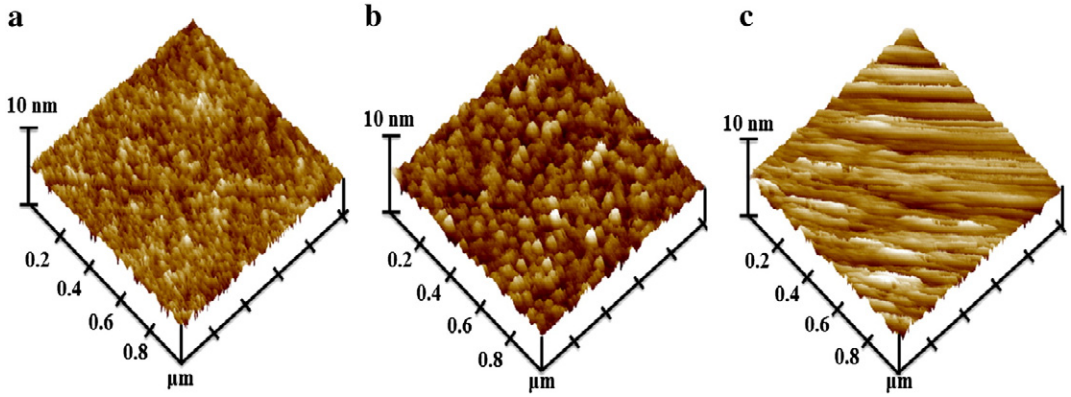

Fig. 4. Three-dimensional height scan images of pure polyimide prepared at the RF magnetron sputtering working pressure of (a) 4 mTorr, (b) 6 mTorr and (c) 8 mTorr. (The thickness of Si_3N_4 barrier film is 100 nm and the power density is 100 W).

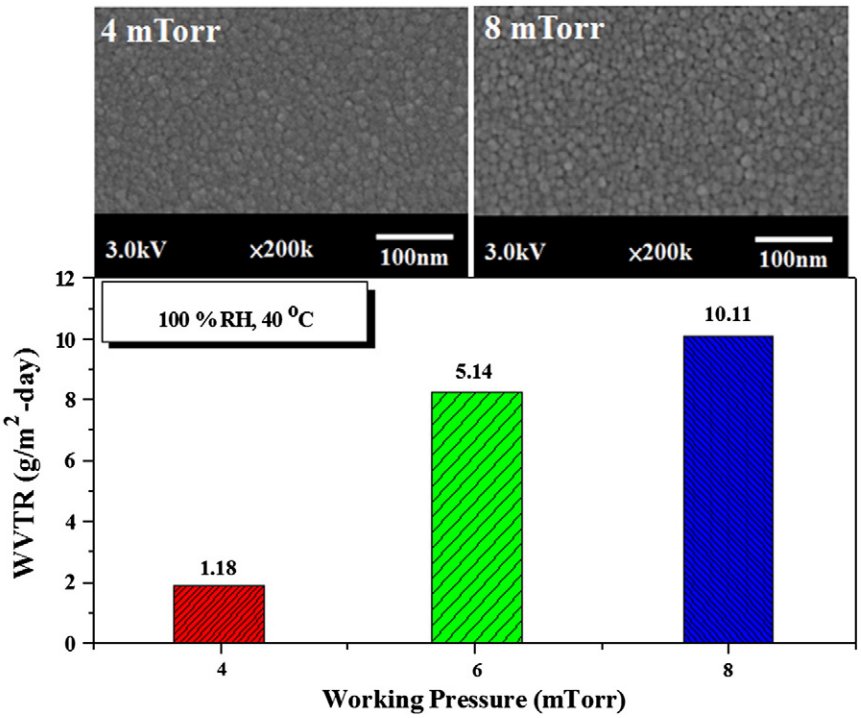

Fig. 5. The WVTR and surface morphologyof Si_3N_4 deposited pure PI in dependence of RF magnetron sputtering with various working pressure: 4 mTorr, 6 mTorr, and 8 mTorr. (The thickness of Si_3N_4 barrier film is 100 nm with 100 W of power density).

In the following discussion, the sputtering power, working pressure and deposited thickness were 100 W, 4 mTorr and 100 nm, respectively. Fig. 6 shows the WVTR of PI and PI/Al_2O_3 hybrid films with various amounts of Al_2O_3 and thicknesses of deposited Si_3N_4. In addition, the effect of bending test, which was conducted up to 8000 times, on the measured WVTR of the Si_3N_4 barrier film (100 nm in thickness) on pure PI and PI/Al_2O_3 hybrid films was also demonstrated in Fig. 6. The results showed that the WVTR of films before Si_3N_4 barrier film deposited increased noticeably with increasing Al_2O_3 content from 0 to 15 wt.%. Upon the deposition of 100-nm-thickness Si_3N_4 barrier films on PI/Al_2O_3 hybrid films, the WVTR reduced dramatically to 2.26, 1.16, 1.48, 2.12, and 5.20 g/m^2-day corresponding to Al_2O_3 content of 0, 4, 6, 10, and 15 wt.%, respectively. The WVTR value of 4 wt.% Al_2O_3–PI hybrid film deposited with 100 nm Si_3N_4 barrier film was the lowest among all Si_3N_4 deposited films before and after the bending test. The high amount of interface bonding, which was evidenced in the following XPS measurements, between Si_3N_4 barrier film and PI/Al_2O_3 hybrid film may be responsible for low WVTR.

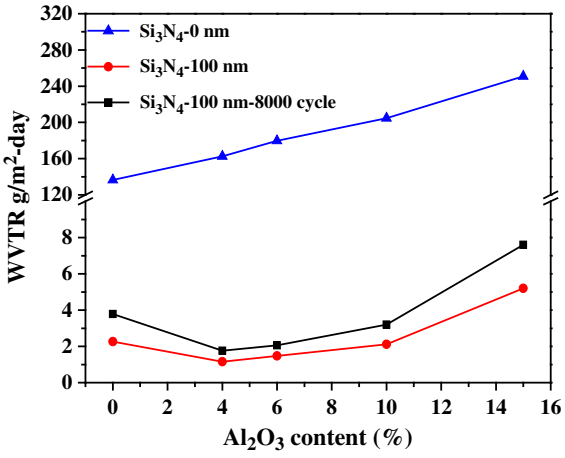

Fig. 6. WVTR of the hybrid films with deposited the Si_3N_4 barrier films before and after bending test of 8000 cycles.

X-ray photoelectron spectroscopy (XPS) was used to study the interface bonding between Si_3N_4 barrier film with 20 nm thickness and 15 wt.% Al_2O_3–PI hybrid film. The thickness of the transition layer between 20 nm-thickness Si_3N_4 barrier film and 15 wt.% Al_2O_3–PI was estimated by using the sputtering rate of the Ar ion, 14.09 nm/min, during XPS depth profiling. And the photoelectron yield was calculated with the composition-depth profiles to exceed the thickness of Si_3N_4 barrier film. Fig. 7 displays the XPS spectra of Al_{2p} and O_{1s} photoelectron emission peaks on the interface between Si_3N_4 barrier film and 15 wt.% Al_2O_3–PI. After curve fitting, three components were found from the Al_{2p} photoelectron peak at approximately 73.5, 74.6 and 76.2 eV, which are respectively attributed to Al–N, Al oxide/hydroxide and Al–O–Si bonds [20]. Moreover, the deconvolution of O_{1s} photoelectron peak by Gaussion curves showed Si–O–Si, Si–O–Al and Al–O–Al peaks and then the existence of bonding at interface was confirmed [21].

4. Conclusion

The PI/Al_2O_3 hybrid films with different Al_2O_3 content were prepared via two steps reaction. The hybrid films obtained by this method exhibited high thermal stability, excellent dimensional stability and mechanical property by the addition of adequate Al_2O_3 content. The Si_3N_4 barrier films had been successfully deposited on pure PI and PI/Al_2O_3 hybrid films via RF magnetron sputtering. The Si_3N_4 barrier film deposited on 4 wt.% Al_2O_3–PI hybrid film at a lower work pressure (4 mTorr) showed a denser structure, lower root mean square (RMS) surface roughness (0.494 nm) and lower transmission rate of water vapor. The WVTR of 4 wt.% Al_2O_3–PI hybrid film deposited with Si_3N_4 (100 nm in thickness) after bending test was 1.76 g/m^2-day compared to 1.16 g/m^2-day before bending. This phenomenon was due to the interface bonding, Al–N and Al–O–Si, between Si_3N_4 barrier film and Al_2O_3–PI hybrid film, which was confirmed with the XPS composition-depth profile.

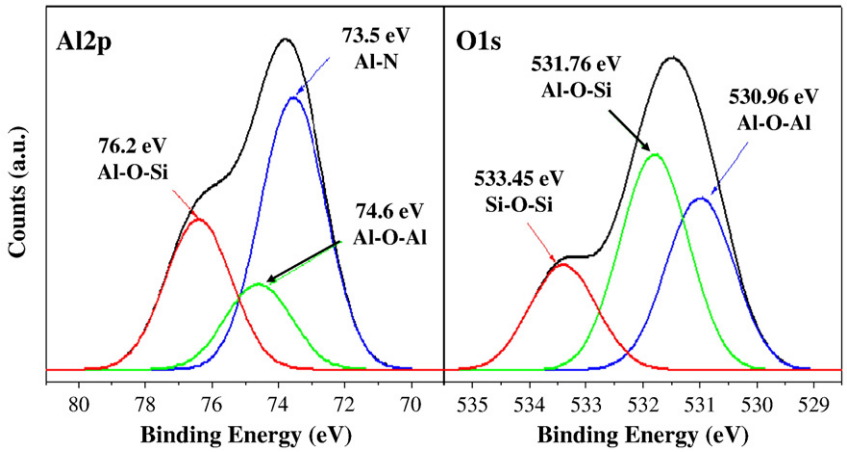

Fig. 7. XPS spectra of Al_{2p} and O_{1s} peaks and the deconvolution results on the interface between Si_3N_4 barrier film and 15 wt.% Al_2O_3–PI hybrid film.

Acknowledgements

The authors would like to acknowledge the financial support of the Ministry of Economic Affairs, Republic of China, Taiwan, through the project on flexible polymeric materials for electronic application (98-EC-17-A-07-S1-120).

References

[1] M.C. Choi, J.C. Hwang, C. Kim, S. Ando, C.S. Ha, J. Polym. Sci. Polym. Chem. 48 (2010) 1806.
[2] C.J. Chang, H.Y. Tzeng, Polymer 47 (2006) 8536.
[3] C.J. Chang, M.S. Wu, P.C. Kao, J. Polym. Sci. Polym. Phys. 45 (2007) 1152.
[4] M.H. Tsai, P.C. Chiang, W.T. Whang, C.J. Ko, S.L. Huang, Surf. Coat. Technol. 200 (2006) 3297.
[5] M.H. Tsai, W.T. Whang, Polymer 42 (2001) 4197.
[6] M.H. Tsai, S.J. Liu, P.C. Chiang, Thin Solid Films 515 (2006) 1126.
[7] M.H. Tsai, W.T. Whang, J. Appl. Polym. Sci. 81 (2001) 2500.
[8] M.H. Tsai, C.J. Ko, Surf. Coat. Technol. 201 (2006) 4367.
[9] K.C. Chang, H.F. Lin, C.Y. Lin, T.H. Kuo, H.H. Huang, S.C. Hsu, J.M. Yen, J.C. Yang, Y.H. Yu, J. Nanosci. Nanotechnol. 8 (2008) 3040.
[10] C. Charton, N. Schiller, M. Fahland, A. Hollander, A. Wedel, K. Noller, Thin Solid Films 502 (2006) 99.
[11] B.M. Henry, A.G. Erlat, A. McGuigan, C.R.M. Grovenor, G.A.D. Briggs, Y. Tsukahara, T. Miyamoto, N. Noguchi, T. Niijima, Thin Solid Films 382 (2001) 194.
[12] M.C. Lin, C.H. Tseng, L.S. Chang, D.S. Wuu, Thin Solid Films 515 (2007) 4596.
[13] C.C. Chiang, D.S. Wuu, H.B. Lin, Y.P. Chen, T.N. Chen, Y.C. Lin, C.C. Wu, W.C. Chen, T.H. Jaw, R.H. Horng, Surf. Coat. Technol. 200 (2006) 5843.
[14] D.S. Wuu, W.C. Lo, C.C. Chiang, H.B. Lin, L.S. Chang, R.H. Horng, C.L. Huang, Y.J. Gao, Surf. Coat. Technol. 198 (2005) 114.
[15] M.C. Lin, L.S. Chang, H.C. Lin, Surf. Coat. Technol. 202 (2008) 5440.
[16] J.H. Chang, D.K. Park, K.J. Ihn, J. Appl. Polym. Sci. 84 (2002) 2294.
[17] D.S. Wuu, T.N. Chen, E. Lay, C.H. Chang, H.F. Wei, L.Y. Jiang, H.U. Lee, Y.Y. Chang, J. Electrochem. Soc. 157 (2010) 47.
[18] W.S. Lau, S. Gunawan, Joy B.H. Tan, B.P. Singh, Microelectron. Reliab. 48 (2008) 187.
[19] C.J. Weng, J.Y. Huang, K.Y. Huang, Y.S. Jhuo, M.H. Tsai, J.M. Yeh, Electrochim. Acta 55 (2010) 8430.
[20] A. Franquet, M. Biesemans, H. Terryn, R. Willem, J. Vereecken, Surf. Interface Anal. 38 (2006) 172.
[21] G.G. Biino, P. Groning, T. Meisel, Meteorit. Planet. Sci. 33 (1998) 89.